INTERNATIONAL JOURNAL OF REFRIGERATION 33 (2010) 1251–1263

available at www.sciencedirect.com

journal homepage: www.elsevier.com/locate/ijrefrig

Nucleate pool boiling, film boiling and single-phase free convection at pressures up to the critical state. Part II: Circumferential variation of the wall superheat for a horizontal 25 mm copper cylinder

Dieter Gorenflo, Elmar Baumhögger, Thorsten Windmann, Gerhard Herres*

Institut für Energie- und Verfahrenstechnik der Universität Paderborn, Warburger Str. 100, D-33098 Paderborn, Germany

Dedicated to Professor Dr.-Ing. Dr.h.c.mult. Karl Stephan on the occasion of his 80th birthday.

ARTICLE INFO

Article history:
Received 5 August 2010
Accepted 10 August 2010
Available online 18 August 2010

Keywords:
Heat transfer
Nucleate boiling
Film boiling
Free convection
Critical state
Horizontal cylinder

ABSTRACT

Transcritical working cycles of refrigerants led to increased interest in heat transfer near the Critical State. In general, experimental results for this region differ significantly from those far from it because some fluid properties vary much more there than at a greater distance. In this paper, two-phase and single-phase free convective heat transfer to refrigerant R125 is discussed for fluid states very close to the Critical Point and far from it. In Part II, circumferential variation of the wall superheat is related to the motion of the fluid within the superheated boundary layer. In nucleate boiling, a minimum in the superheat develops on the lower parts of the wall that can be related to additional evaporation into the bubbles sliding upwards in close contact with the heated wall. In film boiling and supercritical free convection, a slight maximum superheat is discovered on the lower parts of the wall, the *relative* size of which increases close to the Critical Point, while it does not exist in far sub-critical free convection.

Ebullition libre nucléée, ébullition pelliculaire et convection libre monophasique à des pressions allant jusqu'à l'état critique. Partie II : variations circonférentielles de la surchauffe de la paroi d'un cylindre horizontal de 25 mm en cuivre

Mots clés : Transfert de chaleur ; Ébullition libre nucléée ; Ébulliton pelliculaire ; Convection libre ; État critique ; Cylindre horizontal

* *Corresponding author*. Tel.: +49 5251 60 2393; fax: +49 5251 60 3522.
E-mail address: digo@thet.upb.de (D. Gorenflo).
0140-7007/$ – see front matter © 2010 Elsevier Ltd and IIR.
doi:10.1016/j.ijrefrig.2010.08.004

Nomenclature

A	surface area (m^2) of tube or cylinder
CP	critical point
d_B	diameter (mm) of bubbles
p	pressure (bar)
p^*, ρ^*, T^*, v^*	reduced properties
Q	electrical energy input (W)
q	heat flux ($W\,m^{-2}$ or $kW\,m^{-2}$)
q_{max}	maximum heat flux ($kW\,m^{-2}$) in nucleate boiling
q_{min}	minimum heat flux ($kW\,m^{-2}$) in film boiling
R_a	mean roughness height (μm), ISO 4287
T	temperature (°K or °C)
ΔT	superheat or temperature difference (K or mK)
Δt	time interval (ms)
α	heat transfer coefficient ($kW\,m^{-2}\,K^{-1}$)
φ	circumferential or azimuthal angle (°)
ρ	density ($kg\,m^{-3}$)

Indices

c	at critical point
el	electrical
f	fluid state in the pool (far from test tube)
loc	local value
m	mean value
s	at (vapour/liquid) saturation conditions
w	on wall of test tube or cylinder

1. Introduction

Transcritical working cycles for refrigerants have led to increased interest in heat transfer near the Critical State in recent years. Therefore, single-phase and two-phase free convective heat transfer has been measured from an electrically heated horizontal copper tube with 25 mm O.D. to refrigerant R125($CHF_2.CF_3$) for fluid states very close to the Critical Point (CP) and at a greater distance for a wide range of heat fluxes.

The detailed motives of the investigation have been explained in Part I of the paper (Gorenflo et al., 2010) and it has been shown there that integral heat transfer for film boiling slightly below and for free convection slightly above the critical pressure are very similar. In this Part II, circumferential variation of the wall superheat will be analyzed for nucleate boiling, film boiling and single-phase free convection, and it will be related to bubble formation and movement *in nucleate boiling*, and to the motion of the vapour film or superheated fluid around the tube *in film boiling or single-phase convection*, respectively.

In the case of *nucleate boiling*, previous measurements of local heat transfer existed with a horizontal 8 mm copper tube (Bier et al., 1981), with plain and finned steel tubes of large diameter (88 mm O.D.; Buschmeier et al., 1994; Hübner et al., 2001), a stainless steel tube of 15 mm O.D. (Hahne and Barthau, 2006), and the 25 mm copper tube of this investigation (Kotthoff et al., 2006; Kotthoff and Gorenflo, 2009). The new measurements extend the pressure range to higher reduced pressures.

For *film boiling and supercritical free convection*, no data about circumferential variation of the wall superheat could be found. The new experimental results may be useful to improve prediction methods for heat transfer.

2. Experimental procedure

The important features of the experimental equipment and the main principles of the experimental procedure have been explained already in Part I. In the following, measurement and error limits of the superheat ΔT of the tube surface are discussed more in detail because sometimes very small variations of the wall superheat with azimuthal angle φ will be interpreted within the subsequent sections.

The cross section of the tube shown in Fig. 2, Part I has been completed in Fig. 1 by the azimuthal positions of the thermocouples in the two measuring planes, the *main* being situated somewhat on the left of the center of the sight glass (100 mm free diameter) in the evaporator (Fig. 1, Part I, photo) and the *secondary* being axially shifted to the right for 30 mm. Throughout the paper, the data points for the two cross sections are characterized by big (main) or small (secondary) symbols (for the new measurements), as e.g. in Fig. 3.

In 2003, the whole surface of the tube had been sandblasted sequentially with two sizes of Corundum grain, as described in Part I. This resulted in an average value of 0.55 μm for the mean roughness height R_a with comparatively broad size distribution, $0.4 \le R_a \le 0.7$ μm, for individual measuring runs at various locations of the surface, analyzed by Luke (2006) and Kotthoff and Gorenflo (2009).

Then the area containing the main cross section of measurement was rolled reducing R_a to 0.10 μm (roughness analysis in Kotthoff et al. (2006) and Kotthoff and Gorenflo (2009), together with heat transfer results in the latter), and this area was twice sandblasted again in 2006 trying to achieve the same mean roughness height as existing for the secondary cross section. Before starting the new heat transfer experiments in 2008, roughness was measured again resulting in average values of 0.52 μm for the main and 0.51 μm for the secondary cross section (it is likely that the reduction from 0.55 to 0.51 μm was caused by the heat transfer measurements and various cleaning procedures between 2003 and 2008).

For achieving the narrow overall error limits following from some $\Delta T(\varphi)$-sequences for small heat fluxes $q < 1\,kW\,m^{-2}$ (or $< 0.1\,W\,cm^{-2}$, resp.), e.g. in Figs. 3 and 5, various conditions of different kind exist that have been met in the present investigation (and in previous measurements with the same equipment):

(A) Fluctuations of the energy input to the tube were minimized by stabilizing the dc-voltage of the heater and isolating it from the main supply.
(B) Absolute temperatures T_f of the fluid in the pool were measured by resistance thermometers (Pt100) calibrated at regular time intervals. Measurements of saturation

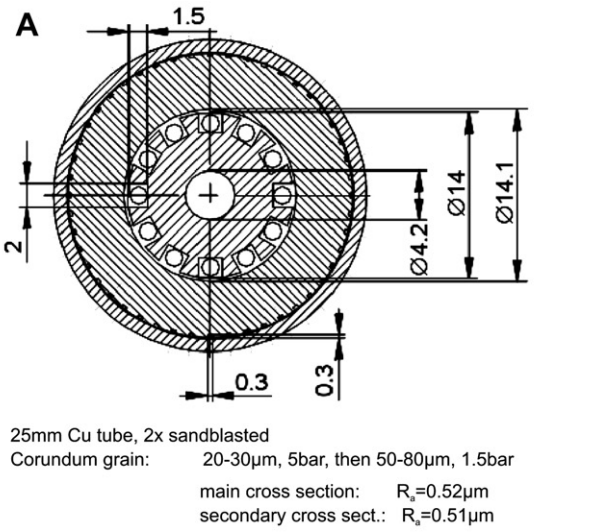

Fig. 1 – A. Cross section of test tube, to scale. B. Detail of test tube, to scale. C. Azimuthal (circumferential) positions of the thermocouples in the two measuring planes.

temperature and pressure were always checked by REFPROP data or other reliable data bases and agreement was within 0.01 K and 0.01 bar or better (for about 25 different fluids investigated during the past decade, cf. e.g. Gorenflo and Kenning, 2010), this mainly demonstrating that no disturbing impurities existed in the pool.

(C) The pool was thermostatted exactly at the saturation temperature corresponding to the constant pressure chosen for a certain experimental run in the case of nucleate or film boiling, and in case of supercritical free convection at the temperature that follows from the Equation of State for density and pressure in the pool. This was realized by sensitive, time-independent adjustment (C,a) of the air temperature in the chamber containing the test loop and (C,b) the temperature of the coolant in the cooling loop – with approaching the temperature of the pool for the smallest heat fluxes investigated and arriving at this temperature for $q = 0$ at the end of the run, see also (F,c). For high heat fluxes, the wall of the tube that returns fluid to the pool can be heated, but this is only necessary in experiments with wide boiling mixtures.

(D) The inner structure of the test tube should not contain any (unknown) local heat transfer resistances. To achieve this, (D,a) all parts of the tube were soft soldered in a glove box under reducing atmosphere to avoid solid oxide particles in the liquid solder, (D,b) having produced before a homogeneous cover of solder on all surfaces to be combined, surfaces of the resistance heater and thermocouples included.

(E) The thermocouples (E,a) have measuring junctions that are insulated from their outer (metal) wall, (E,b) originated from the same production batch, (E,c) have an outer diameter of 0.25 mm and are located in axial grooves of 0.3×0.3 mm to minimize errors in their radial position, and (E,d) after introducing the last in its groove, the cool-down started at the sealed end of the tube, proceeding slowly to the other end (located higher) while liquid solder was permanently supplied to compensate for the shrinking process during solidification.

(F) Treatment of the measuring signals (=thermoelectric voltages): (F,a) To avoid any switches (producing additional thermoelectric voltages) before amplifying the thermoelectric voltage, each thermocouple was provided with its separate amplifier and reference junction in the pool. Each amplifier circuit includes a 0.1 Hz low pass filter to reduce higher frequency noise and the output is connected to a 64 channel 16 bit A/D converter data acquisition board. Samples of all channels are made every second and integrated to a mean value for each channel over approximately 1.5 min (upper diagram of Fig. 2). (F,b) All connections between different metals on the way to the amplifier are mounted in copper blocks and thermostatted in the chamber for the test loop to avoid disturbing thermoelectric voltages. (F,c) All measuring runs ended with heat flux q from the tube approaching zero in steady state conditions, i.e. temperature of the cooling loop arriving at the temperature of the fluid in the pool. Recording of thermocouples continued and reading of each thermocouple at $q = 0$ was used to correct all the readings of this thermocouple during the run, i.e. at $q > 0$.

This is shown in the upper diagram of Fig. 2 for an example at very high reduced pressure ($p^* > 0.96$) with small average $\Delta T \approx 0.02$ K, so the overall scatter of the signals within ± 0.02 K

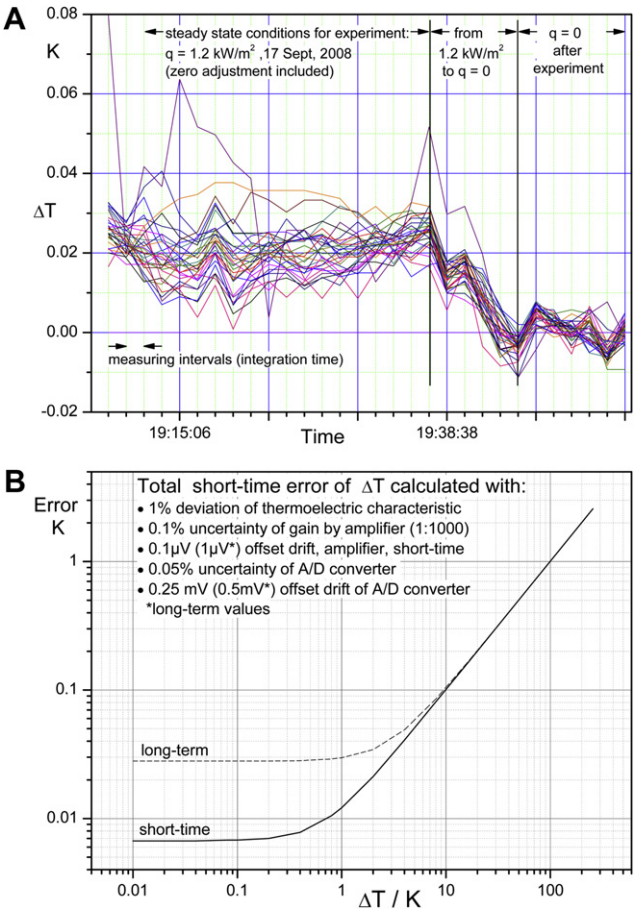

Fig. 2 – Error of ΔT-measurement. Example: R125 and 25 mm Cu-tube. A. Scatter of thermocouple readings for an example with small average $\Delta T \approx 0.02$ K at $p^* > 0.96$. B. Maximum contributions of the components to the "short-time" error ending up at about ±7 mK for $\Delta T < 0.1$ K, including the drifts.

– *containing already the corrections* by the readings at $q = 0$ – and the smaller scatter for each of the thermocouples can be verified. The time interval of approx. 1.5 min between each measurement is needed to perform the sequential measurements (besides $\Delta T_{i\ldots n}$: Pt's 100, pressure transmitter, voltage, current etc.) and used for integration of the signals for each thermocouple; the coloured lines combining the measurements have only been added for easier following the variation of each signal. If the scatter for one or two thermocouples is much higher than for the rest, it will be excluded from the measurement for this data point, e.g. the one with peaks at 0.06 or 0.05 K for 19:15 or 19:37 h, respectively.

In the lower diagram of Fig. 2, the maximum contributions of the components to the error in the ΔT-measurement are listed, which are dominated at high ΔT by the deviation of ±1% from the thermoelectric characteristic and are ending up at about ±7 mK for $\Delta T < 0.1$ K, with "short-time" corresponding to the time needed for an entire run at $p = \text{const}$ (=a few hours).

A final statement should be added about the *history* of the tube: It was manufactured in 2000 and established with 24 thermocouples in the main and 12 in the secondary cross section (and 12 more equidistant grooves without thermocouples to achieve total symmetry, Fig. 1). In the meantime, 7 different surface finishes have been applied and removed (except the final), three of them containing patterns of macrocavities (200 × 100 × 50 microns, each) manufactured by Wieland Company, Ulm.

As a result, the outer diameter decreased from 25.4 to 25.0 mm, and in the handling connected with the various modifications, six thermocouples in the main and one in the secondary cross section have been "lost". This can be verified by a closer look at the $\Delta T(\varphi)$-sequences of Fig. 3, because the diagrams in column (B) originate from measurements with the first (fine sandblasted) surface treatment containing all 24 and 12 thermocouples, and those in column (A) originate from the last (actual) measurements with R125 and the twice sandblasted surface, where data of the φ-locations at 30, 105, 120, 165, 195, 225, and 232.5° are missing. (In Kotthoff et al., 2006), four more thermocouples in the secondary cross section were reported defective, but their problems were caused by defects in connections external to the thermocouple and were subsequently repaired.)

3. Nucleate boiling

Variation of *local* wall superheat ΔT with circumferential angle φ has been investigated with this tube in the past quite extensively for **nucleate boiling** of R134a, Propane and 2-Propanol on various surface modifications, see e.g. the summary in Kotthoff et al. (2006) and more recently Kotthoff and Gorenflo (2009).

The new measurements with R125 shown for a wide range of heat fluxes at constant, *intermediate* reduced pressure $p^* = 0.2$ in Fig. 3 (column (A) of the diagrams), confirm the previous results, samples of which are given in column (B) with linked photos in column (C). There is a minimum of ΔT at the bottom of the tube for intermediate densities of active nucleation sites (i.e. intermediate heat fluxes and reduced pressures) caused by evaporative and convective *enhancement of heat transfer* due to bubbles originating from nucleation sites on the lower parts of the tube and sliding upwards in close contact with the superheated liquid layer near the wall.

The minimum of ΔT extends more or less over the entire lower half of the tube and the sequence of data points meets the dot–dashed horizontal lines in the middle of the circumference (90 or 270°) – for all heat fluxes with a ΔT-minimum in this column-, which indicate the average ΔT-values for the two cross sections and were used in the definition of the heat transfer coefficients α discussed in Part I of the paper.

A detailed comparison of the $\Delta T(\varphi)$-sequences for the main and secondary cross sections in column (A) of Fig. 3 reveals

- that the sequences for $q = 0.1\ \text{kW m}^{-2}$ without bubble formation coincide within a few mK,
- that only a very slight tendency to form a ΔT-minimum exists for the secondary cross section at 0.3 and $1\ \text{kW m}^{-2}$, whereas the minimum can already be recognized quite well for the main cross section at these heat fluxes; it seems that less bubbles are formed on the lower parts of the tube in the

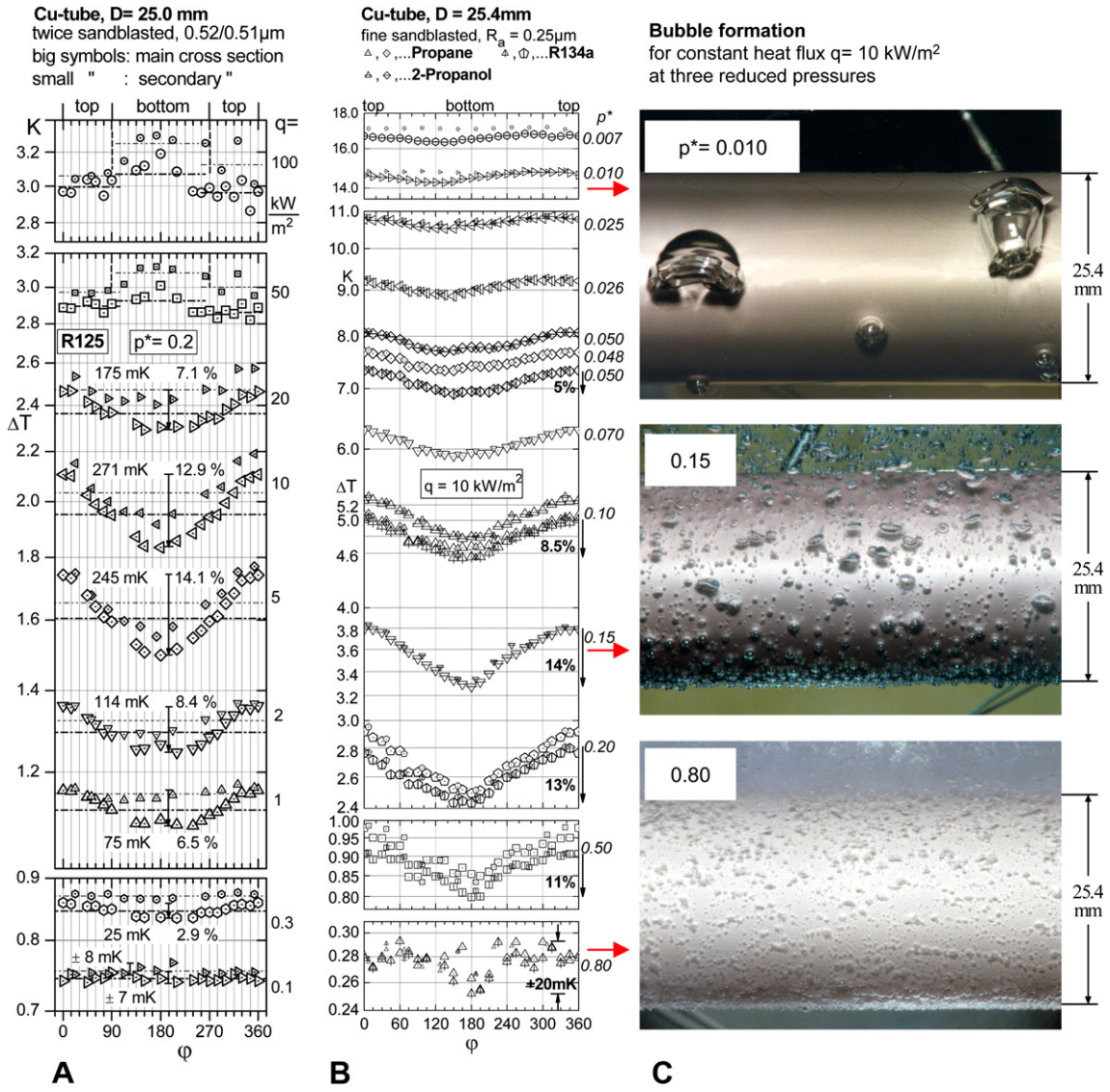

Fig. 3 – Variation of local wall superheat with circumferential angle φ (A), (B), and examples of bubble formation (C) on a 25 mm Cu-tube (B, C acc. to Kotthoff et al., 2006, mod.). A. New data for R125($CHF_2.CF_3$) on twice sandblasted surface: Variation of heat flux q at constant intermediate reduced pressure $p^* = 0.2$. B. Earlier data for 3 fluids on fine sandblasted surface: Variation of reduced pressure p^* at constant intermediate heat flux $q = 10\ kW\,m^{-2}$. C. Bubble formation for 3 reduced pressures at $q = 10\ kW\,m^{-2}$ on fine sandblasted surface (lower two p^*: 2-propanol, highest p^*: R134a).

first case, which are not sufficient to reduce ΔT significantly by the additional heat transfer connected with the sliding process, and

- that the average ΔT is higher for the secondary cross section at all heat fluxes up to the highest, with differences continuously increasing from 11mK or 1.5% (without bubble formation) to 148 mK or 4.9%, except for $q = 2 kW\,m^{-2}$ where it is slightly smaller than for *both* neighbouring q-values. (The sizes in % are always related to the bases of the arrows.) The reason might be that there are somewhat less cavities suitable for bubble formation at small reduced pressures within the roughness scatter near the secondary cross section than near the main – despite the almost identical R_a-values – while this is not the case at high reduced pressures (Fig. 5). It shows again that a single roughness parameter is not sufficient to describe the influence of the roughness pattern on the heated wall in nucleate boiling (cf. e.g. Kotthoff and Gorenflo, 2009).

For all measurements with significant azimuthal variation of ΔT, *the true local* heat fluxes to the surface of the tube will differ markedly from the q-values given on the right side of the diagrams, calculated by $q = q_{el} = Q_{el}/A$, due to azimuthal heat conduction within the cylinder (entirely filled with copper), that will cause heat flow within the wall from the top to the bottom of the tube and *reduce* the heat flux to the surface at the

top, while *increasing* it at the bottom. This has been shown by calculations in Kaupmann (1999) and Danger (2004). For a difference of ca. 5% in ΔT between minimum and average value, the limits are $0.5 \le q_{loc}/q_{el} \le 1.3$ and $0.45 \le \alpha_{loc}/\alpha_m \le 1.35$ (see e.g. the summary in Kotthoff et al., 2006).

The *integral* heat transfer coefficients α discussed in Part I, however, vary only a few percent (less than 3% for ΔT-differences < 20%), if calculation for the $\Delta T(\varphi)$-sequences with minimum is based on purely radial heat flow or on the true local q-variation, respectively (Kaupmann, 1999). Therefore, calculation of heat transfer coefficients by $q = \text{const} = q_{el}$ has not been modified in Part I for simplicity reasons.

A quantitative example of the additional evaporation into the sliding bubbles that continues almost up to the middle of the tube (90 or 270°) is given in Fig. 4 (from Kotthoff and Gorenflo, 2009) for four bubbles originating from nucleation sites located about 2–4 mm below the middle (270°). It demonstrates that the growth rate after departure remains approximately the same as before (open or closed symbols, where departure is defined as lateral (=upward) movement of rear of bubble away from nucleation site). This underlines the important "direct" contribution of sliding bubbles to heat transfer besides their (indirect) contribution by site seeding (Kotthoff and Gorenflo, 2009) and enhanced convection in the wake (Kenning and Bustnes, 2009).

The enhancement of heat transfer vanishes as soon as the bubbles lose contact with the superheated boundary layer near the wall, as is assumed to have happened for the last 20 ms in case of the bubble tracked almost to the middle of the tube (squares) because it does not grow further in this time period (similarly for the last 6 ms in case of the rhombs). And on the *upper* half of the tube, this kind of enhancement does not exist at all.

It loses importance also on the *lower* half and the minimum in ΔT disappears, if the density of active sites becomes high ($q > 20\ \text{kW m}^{-2}$, upper two heat fluxes in column (A) of Fig. 3)

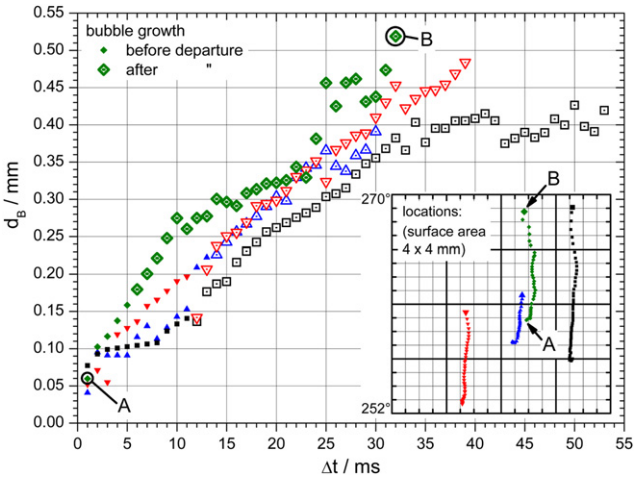

Fig. 4 – Examples of additional evaporation into bubbles sliding upward slightly below the middle of the tube (270°). 2-propanol on 25 mm Cu-tube with twice sandblasted surface, $p^* = 0.1$, $q = 5\ \text{kW m}^{-2}$; from Kotthoff and Gorenflo (2009).

or the number of bubbles becomes small ($q \le 0.3\ \text{kW m}^{-2}$, lowest two heat fluxes).

A detailed comparison of the data for the two highest heat fluxes (100 and 50 kW m^{-2}) reveals that the ΔT-values on the lower half of the tube are slightly *higher* than on the upper as follows from the *average* superheat being ca. 70 or 110 mK (ca. 2.5 or 3.5%) higher than for the upper half in case of $q = 100\ \text{kW m}^{-2}$ (dot–dashed lines).This might be caused by accumulation of bubbles in the dense layer below the tube which prevent enough liquid at T_s to penetrate to the tube surface and slightly increase the superheat of the wall and its immediate vicinity. For $q = 50\ \text{kW m}^{-2}$, the effect is reduced to ca. 60 or 30 mK (ca. 2 or 1% of the average ΔT), and at 20 kW m^{-2}, the minimum starts to be developed.

The same tendency as for the two *lowest* heat fluxes (0.3 and 0.1 kW m^{-2}) at constant (intermediate) $p^* = 0.2$ also exists for constant *intermediate* heat flux $q = 10\ \text{kW m}^{-2}$, if reduced pressure p^* *is very low*, because the number of active sites is small, even at 10 kW m^{-2}, and the bubbles are becoming very big due to very thick boundary layer and high superheat ($\Delta T > 14$ K) as shown in the upper diagram of column (B) and in the upper photo of Fig. 3 for $p^* = 0.01$ from Kotthoff et al. (2006); the data in (B) and the photos have been taken from the previous paper because p^* was varied to much lower values there than in the new experiments with R125 and because heat transfer and bubble formation will qualitatively be the same for the four fluids of Fig. 3 *at the same values of* q *and* p^*.

The minimum in ΔT also disappears, *if* p^* *becomes very high* because of the low buoyancy, tiny bubbles, and high site density (even at small q-values) existing at high p^*, as shown in the lowest photo and the diagram for $p^* = 0.80$ at the bottom of column (B), with an overall scatter of ΔT within ±20 mK.

The influence of heat flux on the circumferential variations of ΔT at high p^* is shown in detail for R125 in Fig. 5. In the left-hand column at $p^* = 0.80$, the scatter is more or less the same for *all* heat fluxes, except for $q = 50\ \text{kW m}^{-2}$ where it is markedly higher and there is a maximum in ΔT at the bottom of the tube.

From these data, it had been concluded in the past that the trend found up to $p^* = 0.80$ would continue at higher reduced pressures. This, however, is not the case as demonstrated by the clear minima in the $\Delta T(\varphi)$-sequences for the four lower heat fluxes between 0.25 and 2 kW m^{-2} at $p^* = 0.90$ in Fig. 5. At $p^* = 0.93$, the outcome of the new measurements is similar (Windmann, 2008), while the effect tends to disappear at $p^* = 0.96$ and has vanished in the overall scatter of between ±6 mK and ±10 mK in the very small values of ΔT for the five heat fluxes measured in nucleate boiling at $p^* = 0.99$.

The effect can be explained using the photos of R125 at $p^* = 0.90$ in Fig. 6, top and middle: On the left, the camera was brought into focus at the plane containing the highest axial line of the tube, and the many very tiny bubbles are visible that are produced there and rise. Two of the biggest – by far – are shown in front of the Pt 100 thermometer in the upper photo on the left, with a hair for comparison (=Fig. 4 of Part I).

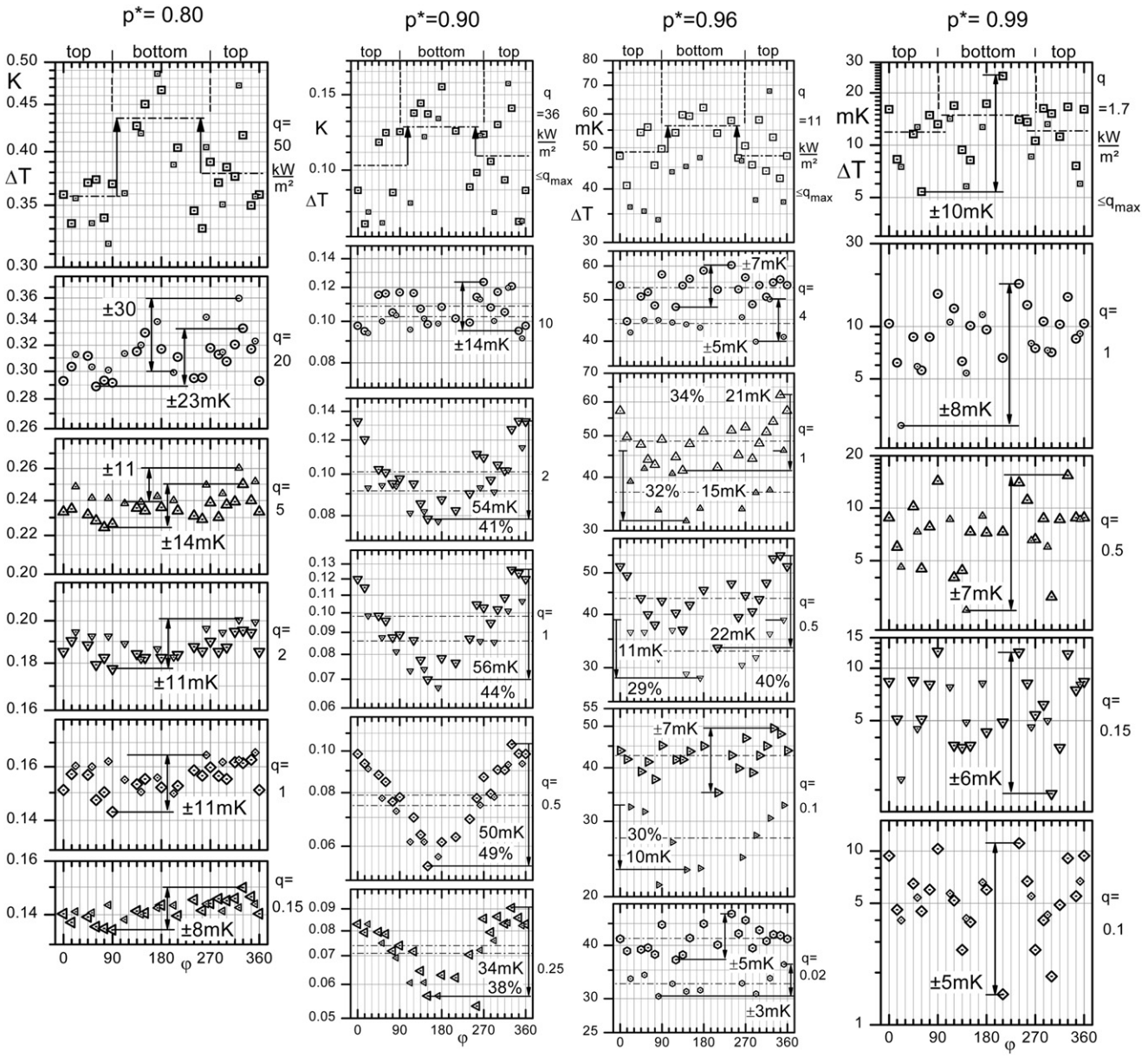

Fig. 5 – ΔT(φ)-sequences in nucleate boiling for a wide range of heat fluxes q at 4 high reduced pressures p^* (R125 on 25 mm Cu-tube).

On the right, the camera was focussed 9 mm in front of that plane showing much larger bubbles within the outer edge of the rising swarm (contracting above the tube), that are coming from the bottom of the tube. Slightly larger bubbles than for 20 W m^{-2} can be seen for the higher heat flux $q = 0.1$kW m^{-2} in the middle, and the bubbles rising from below are even larger for 1 and 5 kW m^{-2} at the bottom of Fig. 6 ($p^* = 0.90$ for all photos of this figure).

The large bubbles that drive the whole swarm (from its outer edge) were produced at the bottom of the tube because growing time at the active nucleation sites and the time for sliding upward are prolonged by small buoyancy, and agglomeration in the upward slide is enhanced by small surface tension. On the other hand, turbulent fluctuations are suppressed (also by small buoyancy), resulting in slow, laminar, strictly parallel motion of the bubbles, without disturbing the circumferential ΔT-pattern.

In the same way as at the intermediate reduced pressure $p^* = 0.2$ (Fig. 3A), the enhancement of heat transfer by the sliding bubbles loses importance for higher heat fluxes also in the pressure range between 90 and 96% of p_c – seen at $q = 10$ kW m^{-2} for $p^* = 0.90$ or already at 4 kW m^{-2} for $p^* = 0.96$ – because the density of active sites becomes higher on the entire heated surface and prevents the rising bubbles from contacting the wall or even the (very thin) superheated liquid layer in the boundary.

And at heat fluxes very close to q_{max} in the highest diagrams of Fig. 5, the ΔT(φ)-sequences reveal the tendency that has been analyzed in Fig. 3 already, with slightly *higher* ΔT's on the lower parts of the tube than on the upper (arrows

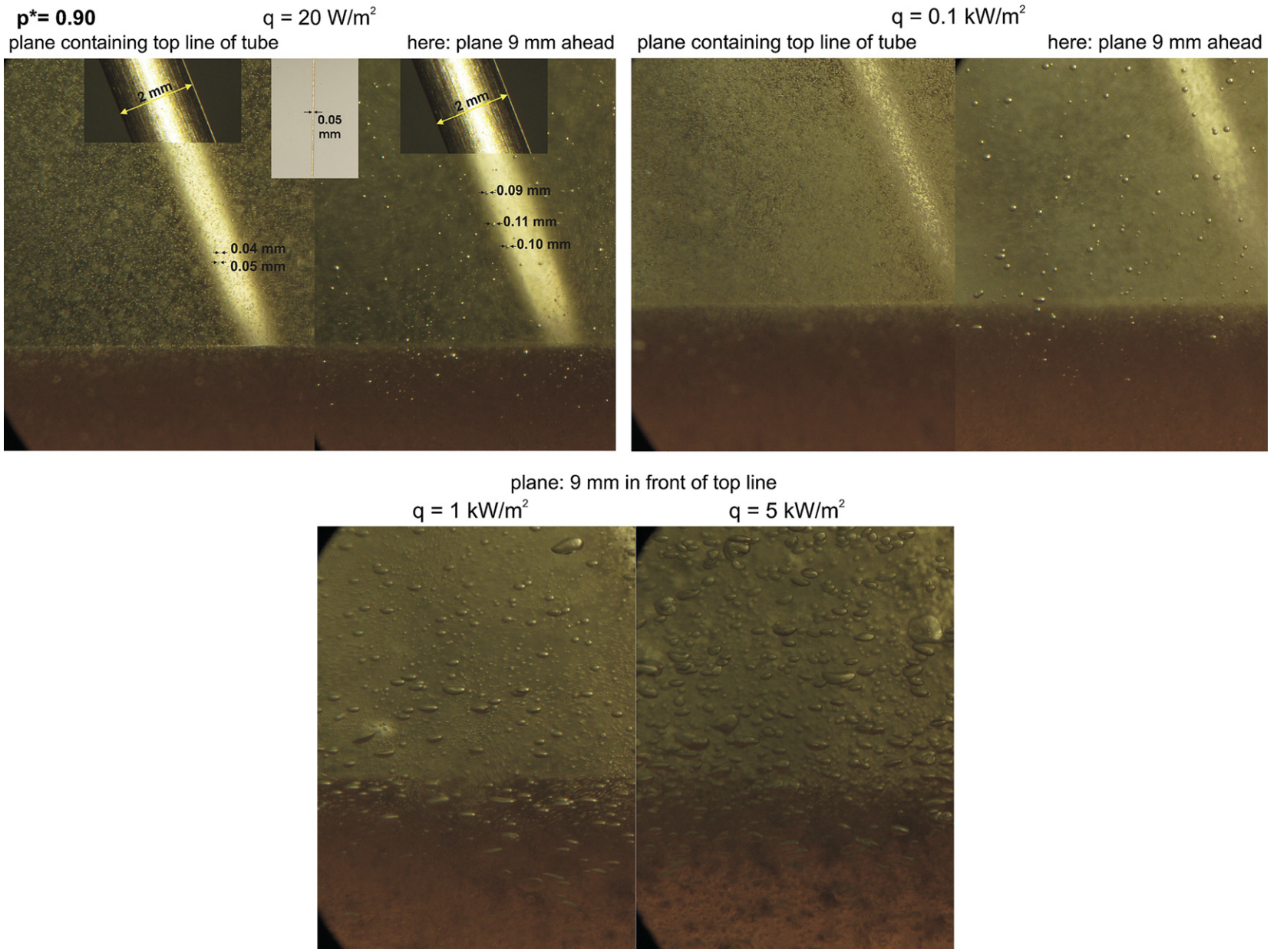

Fig. 6 – Bubble formation in nucleate boiling for 4 heat fluxes q at $p^* = 0.90$ (R125, 25 mm Cu-tube). Top and middle: Comparison of tiny bubbles originating from the top of the tube (on the left) with larger bubbles coming from the bottom (on the right). Lowest Photos: Two higher heat fluxes.

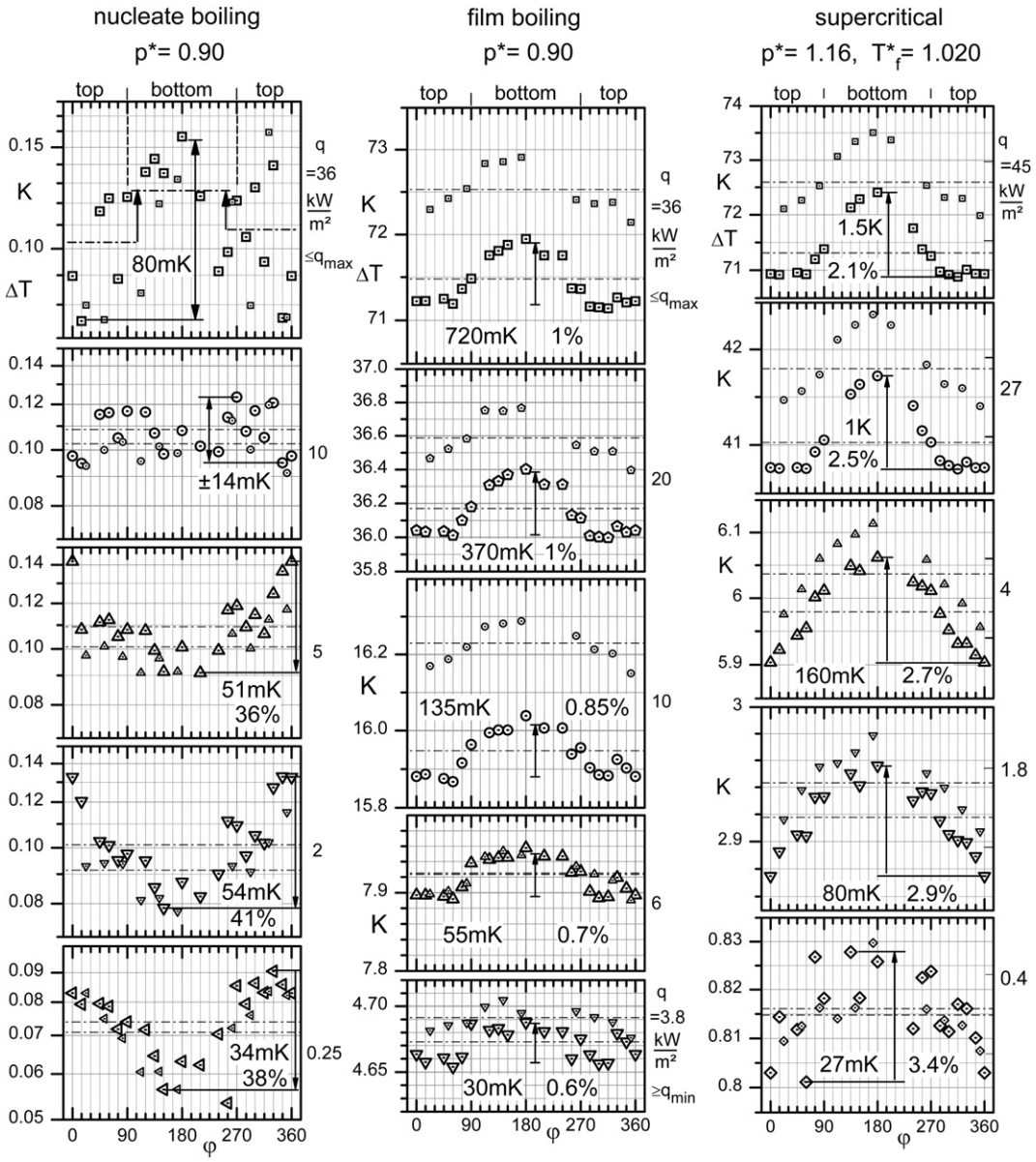

Fig. 7 – ΔT(φ)-sequences in nucleate boiling, film boiling and supercritical free convection at constant reduced pressures p^* for a wide range of heat fluxes q (R125 on 25 mm Cu-tube).

pointing upward) due to accumulation of bubbles in the dense layer below the tube preventing enough liquid at T_s from reaching the tube surface. The effect decreases from 50 mK or more at $p^* = 0.80$ to 7 or 8 mK at $p^* = 0.96$, and it has (almost) vanished at $p^* = 0.99$.

4. Film boiling and single-phase free convection

In Fig. 7, some of the heat fluxes measured for nucleate boiling of R125 at $p^* = 0.90$ are compared with **film boiling** from slightly below q_{max} (=maximum heat flux of nucleate boiling) to slightly above q_{min} (=minimum heat flux of film boiling, cf. e.g. Fig. 6, Part I) at the same pressure and with **supercritical free convection** at the highest pressure investigated, $p^* = 1.16$, but over a range of heat fluxes about ten times wider than between q_{max} and q_{min}.

In both cases, a *maximum* of ΔT is clearly visible now near the bottom of the tube, with a much smaller *relative* extent, however, than for the minimum in nucleate boiling at $p^* = 0.90$. Its magnitude of about 1% remains more or less constant, until q_{min} is approached for film boiling, and the same also holds for supercritical free convection at $p^* = 1.16$, only with a somewhat higher relative extent of 2–3% and a tendency to *increase* (from 2.1 to 3.4%), while it is *decreasing* in film boiling (from 1 to 0.7 or 0.6%) as follows from comparing the middle and right-hand columns of Fig. 7.

This implies that the *absolute* amounts of the peaks decrease more or less in the same way as the superheats ΔT themselves. The pattern with approximately constant ΔT on (almost) the entire upper half of the tube and a peak at the

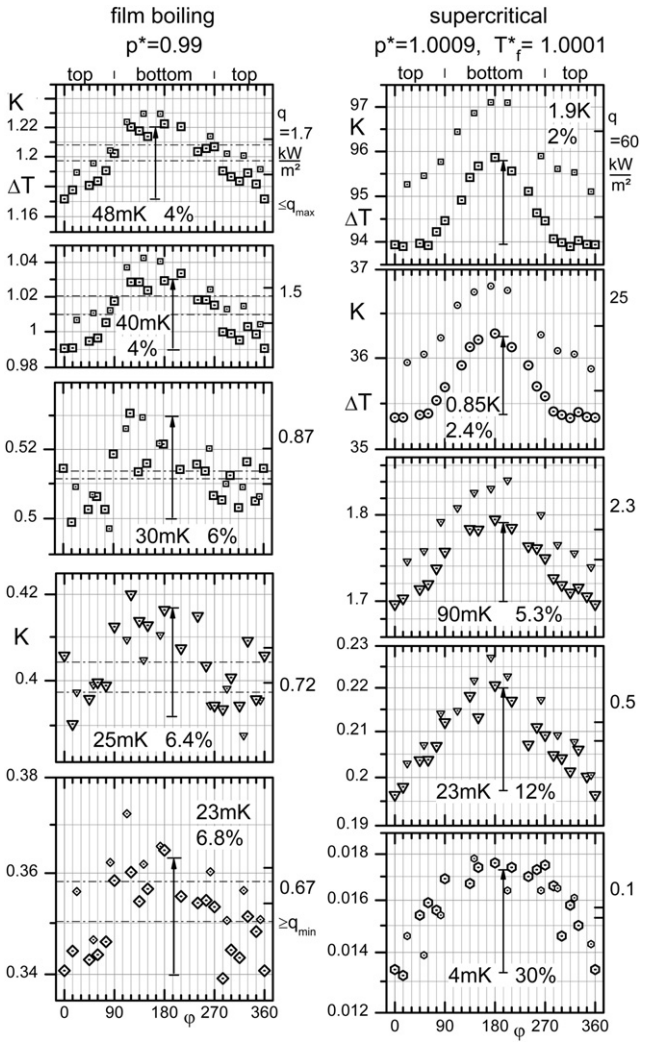

Fig. 8 – ΔT(φ)-sequences in film boiling and supercritical free convection for two reduced pressures p^* close to the Critical Point and various heat fluxes q (R125 on 25 mm Cu-tube).

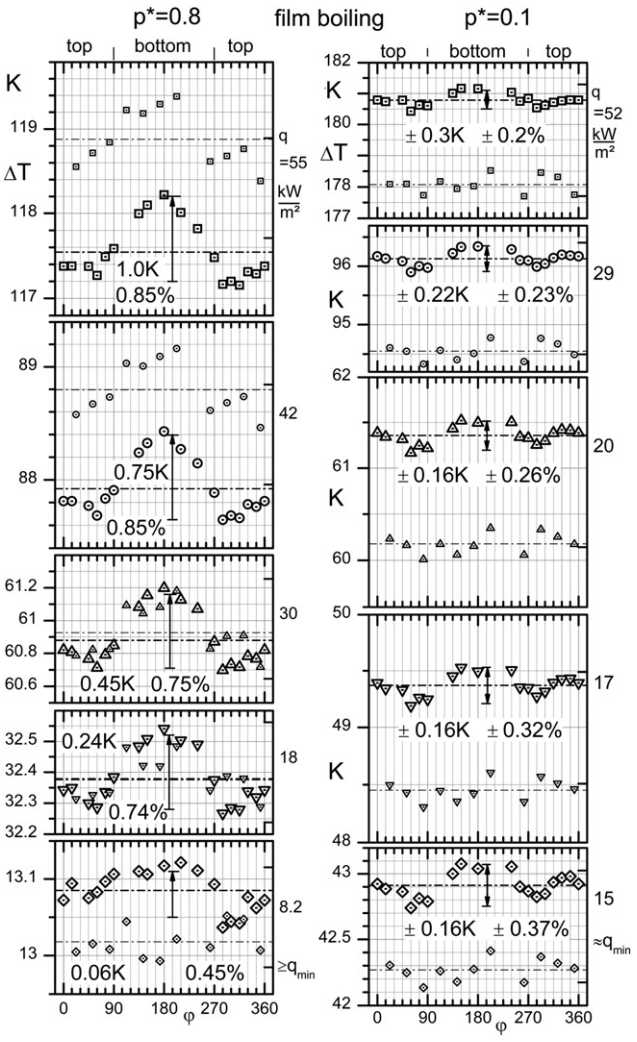

Fig. 9 – ΔT(φ)-sequences in film boiling for a high or low reduced pressure p^* and various heat fluxes down to q_{min} (R125 on 25 mm Cu-tube).

bottom also prevails for supercritical fluid and film boiling closer to CP ($p^* = 1.0009$ and 0.99, Fig. 8) and for film boiling at lower reduced pressures ($p^* = 0.8$ and 0.1, Fig. 9).

While the shape of the $\Delta T(\varphi)$-sequences originating from the two measuring cross sections (at 30 mm axial distance) is very similar for all data in Figs. 7–9 at the same heat flux and pressure, there is a systematic increase of ΔT of about 1–2% at the secondary cross section compared to the main *for high heat fluxes* and all pressures in supercritical free convection or $p^* \geq 0.8$ in film boiling, that disappears towards low q-values.

In Figs. 6 and 14 of Part I, this has caused the small symbols to be shifted to slightly higher ΔT, but remaining *within* the big ones. For q near q_{min} at $p^* = 0.8$ and all heat fluxes at $p^* = 0.1$, however, the situation is vice versa. The reason for these differences has not yet been found.

The $\Delta T(\varphi)$-patterns in Figs. 7–9 can be explained using the photos in Fig. 10 (columns on the left and in the middle): As can be concluded from the irregular wavy structure of the vapour–liquid interface on the upper half of the tube *in film boiling*, the film will be turbulent on this part of the heated surface, and the accumulation of vapour near the top of the tube does not lead to additional heat transfer resistance because of the vigorous motion induced there by the "bubbly" release of the vapour from the wall (with the form and size of these bubbles highly differing from those in nucleate boiling at the same conditions shown for comparison in the column on the right).

With increasing heat flux, the wavy structure of the interface develops lower down the tube (cf. the two heat fluxes at $p^* = 0.10$ and 0.45), but near the bottom of the tube ($180 \pm 45°$), the upward motion of the vapour film starts in laminar form causing a slightly thicker layer of vapour combined with additional heat transfer resistance.

In the case of *supercritical free convection*, turbulent clusters of the fluid are also formed on the upper half of the tube for high heat fluxes (photos for $p^* = 1.16$ and 1.024 at the bottom of Fig. 10) causing the same pattern of the $\Delta T(\varphi)$-sequences as in film boiling. Approaching CP further, as e.g. for $p^* = 1.0009$ in Fig. 8, the structure of the boundary layer around the tube cannot be distinguished any longer in the photos due to critical opalescence of the fluid *in the pool* – while the state in the

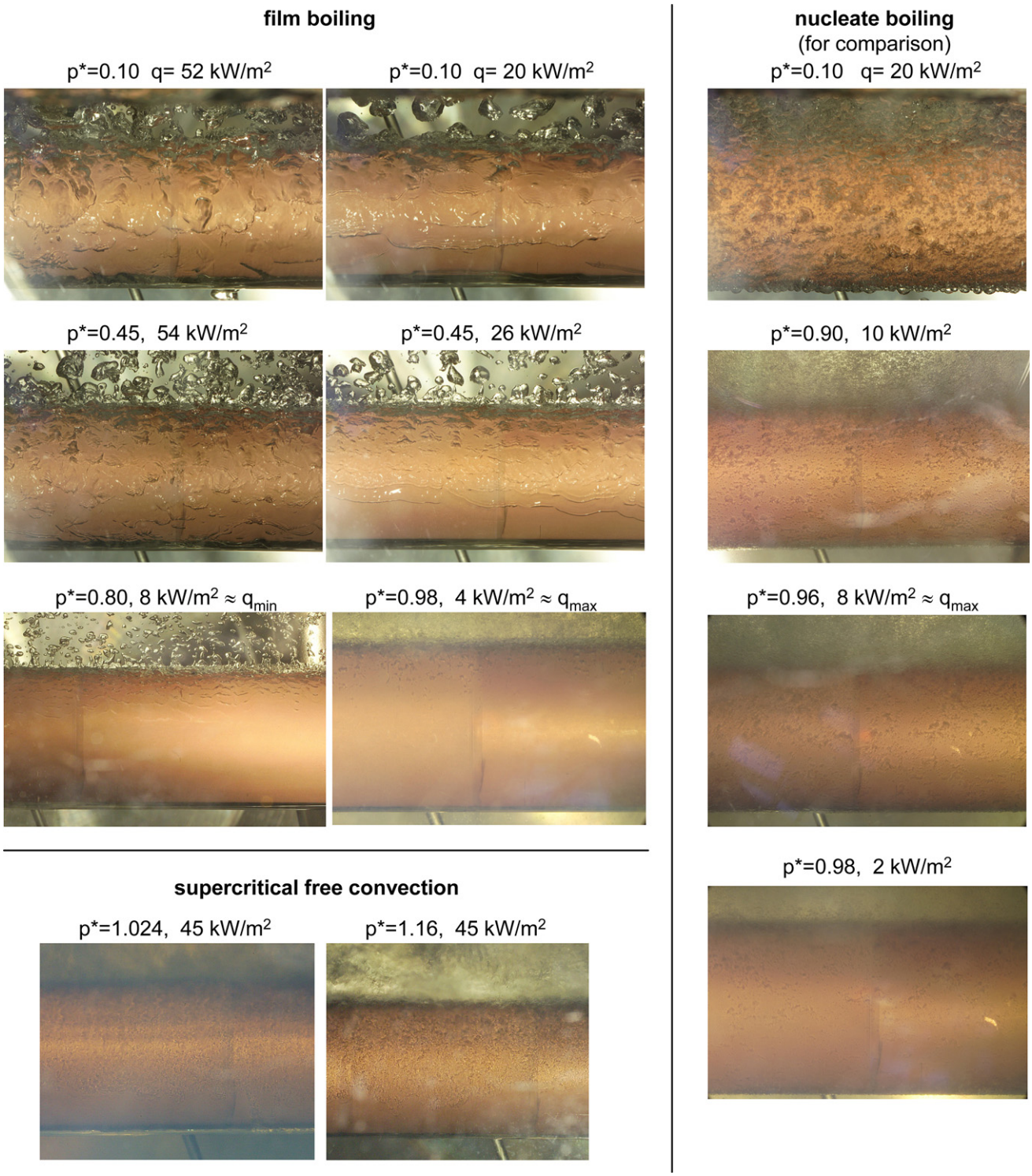

Fig. 10 – Photos of film boiling and supercritical free convection at various heat fluxes and reduced pressures in comparison with nucleate boiling (R125 on 25 mm Cu-tube).

boundary layer is *far* supercritical as follows from $\Delta T > 30$ K for $q \geq 25\text{kW m}^{-2}$ in Fig. 8.

Different from the two highest heat fluxes in supercritical free convection in Figs. 7 and 8, ΔT is not constant any longer on the upper parts of the tube for the three smaller heat fluxes in the columns on the right. Instead, the (parabolic) peaks extend over the entire surface of the tube indicating that the motion of the fluid remains strictly laminar – as can also be concluded from the comparatively narrow scatter within the $\Delta T(\varphi)$-sequences.

For the two smallest heat fluxes in Fig. 8 on the right, the *relative* extent of the peaks increases to 12 and up to 30% – despite the small absolute ΔT-variation of 23 or 4 mK – because the fluid state within the boundary layer passes CP in very close vicinity along the isobar $p = p_c + 33$ mbar – that is

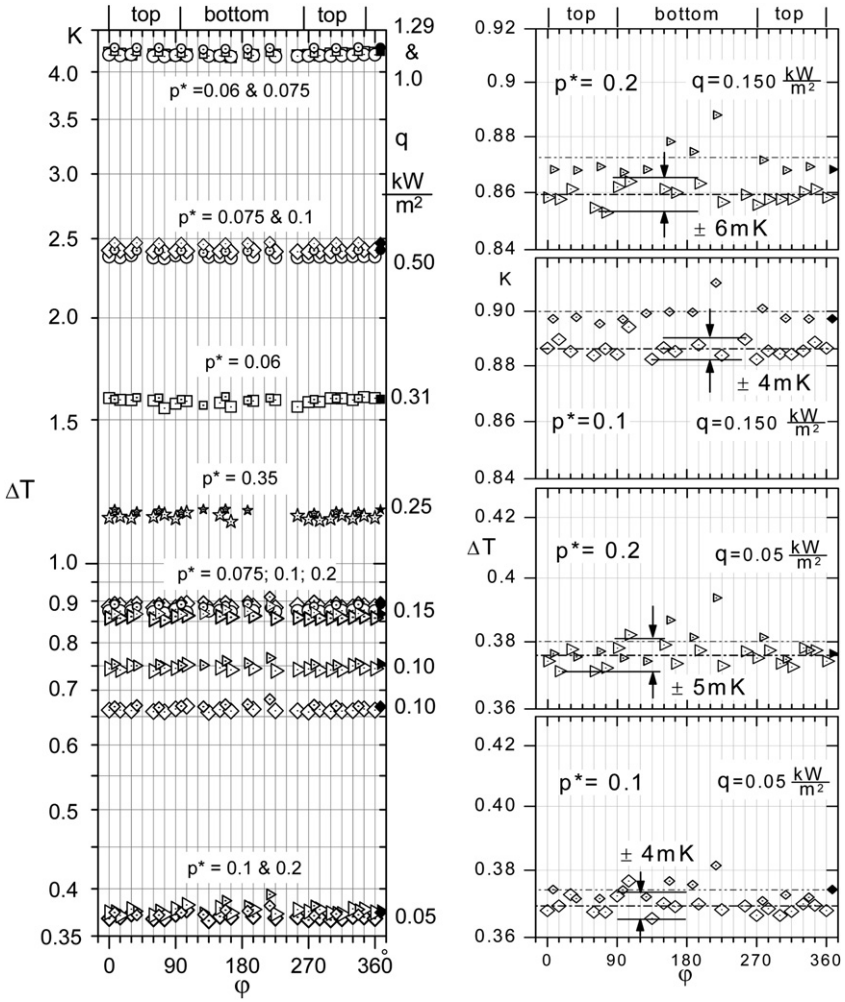

Fig. 11 – All $\Delta T(\varphi)$-data existing on far sub-critical single-phase free convection with R125 and the 25 mm-tube (from Ninkovic, 2008; these data contain an error of $+15^\circ$ in φ for each thermocouple, that has been removed in the preceding diagrams).

identical to the isotherm $T = T_c + 34$ mK, except for a few percent of the thickness of the layer close to the heated wall in the last case (cf. the isobar $p^* = 1.0009$ with the isotherm $T^* = 1.0001$ in Fig. 16, Part I) – resulting in (tremendous) density variation from $\rho_f = 1.05$, $\rho_c = 603\ \mathrm{kg\,m^{-3}}$ in the pool or the outer parts of the boundary layer to $\rho_w = \rho(T_f + \Delta T) = 514\ \mathrm{kg\,m^{-3}}$ for the fluid in contact with the heated wall (using the intermediate $\Delta T = 15$ mK for the example).

The tendency for the peak to disappear *in film boiling* as q_{min} is approached, results from fluctuations in the vapour film that occur shortly before the coherent vapour layer around the tube is breaking down. This can be verified in the lowest diagrams (for film boiling) in Figs. 7–9, if compared to the $\Delta T(\varphi)$-sequences at higher heat fluxes (it also holds for the two heat fluxes of 0.72 and 0.87 $\mathrm{kW\,m^{-2}}$ at $p^* = 0.99$ in Fig. 8 which are not far above q_{min}).

At $p^* = 0.1$ which is the lowest reduced pressure investigated in film boiling, the shape of the $\Delta T(\varphi)$-sequences differs significantly from those at high p^*, as follows from Fig. 9, on the right: Although the tendency towards constant ΔT on the upper parts of the tube remains unchanged due to wavy structure and turbulence in the vapour film (Fig. 10), the ΔT-maximum at the bottom of the tube is reduced to less than 0.4% for all heat fluxes, and minima of the same extent occur on the flanks (90 and 270°).

It seems that the high acceleration of the upward flow of vapour along the flanks, caused by the large density difference between vapour and liquid at this low pressure ($p_s = 3.6$ bar) diminishes the thickness of the vapour layer on the flanks and results in slightly better heat transfer than at the bottom – and even on the upper parts of the surface despite the vigorous motion which is connected with the bubbly release of vapour there. At this pressure, no tendency can be seen that the $\Delta T(\varphi)$-pattern changes near q_{min} (although the measured heat flux $q = 15.005\ \mathrm{kW\,m^{-2}}$ is identical with q_{min} in this case because transition to nucleate boiling was triggered by a very small increase of the pressure (a few mbar) after hours of stationary conditions without any manipulations during an automatic run at night).

In Fig. 11, all $\Delta T(\varphi)$-data existing on far sub-critical single-phase free convection with R125 and the 25 mm-tube (Ninkovic, 2008) are shown for comparison with the new measurements for supercritical fluid states and film boiling. The results agree with many previous experiments with the

same tube and other fluids (Kotthoff et al., 2006; Kotthoff and Gorenflo, 2009) and demonstrate that for far sub-critical liquids, ΔT is constant throughout the circumference of the tube. This holds not only for the small heat fluxes in the enlarged diagrams on the right, but also for the other measurements (data files in Ninkovic, 2008; Kotthoff, 2010).

It indicates that the ΔT-pattern which has been found for supercritical free convection and which is similar to the one in film boiling is caused by the far more pronounced variation of thermophysical properties (particularly density and specific enthalpy) in this region of the fluid state than for (saturated) liquids at low to intermediate reduced pressures.

5. Conclusions

Circumferential variation of the wall superheat ΔT for a horizontal 25 mm copper cylinder in nucleate pool boiling, film boiling and single-phase free convection of the refrigerant R125 has been measured and related to the motion of the fluid within the superheated boundary layer.

In **nucleate pool boiling** on horizontal tubes, a *minimum* in the superheat develops on the lower parts of the wall that had been found earlier for intermediate densities of active nucleation sites, i.e. intermediate reduced pressures and intermediate heat fluxes and can be related to additional evaporation into the bubbles sliding upwards in close contact with the heated wall. The minimum superheat does not exist at small densities of active nucleation sites because the contribution of sliding bubbles to the overall heat transfer is negligible, and it loses importance at very high densities of active sites – high heat fluxes or high reduced pressures – because the heated wall is entirely covered with growing bubbles and the bubbles rising from below do not get in contact with the wall or superheated boundary layer.

For the new measurements at pressures of 90% of the critical pressure or more, the ΔT-minimum develops again due to the bubbles being very tiny (small surface tension) and their motion being very slow and therefore strictly laminar (small buoyancy) so the minimum in the circumferential ΔT-pattern is not disturbed. It disappears only at very high heat fluxes and converts to a maximum in ΔT very close to q_{max} because the bubbles accumulate at the bottom of the cylinder, also due to the small buoyancy.

In **film boiling** and also in **supercritical free convection**, a slight maximum superheat is discovered on the lower parts of the wall, because heat transfer is better on the upper parts produced by turbulence in the superheated layer near the wall. The *relative* amount of the ΔT-maximum increases very close to the Critical Point due to the great variation of thermophysical properties, even for small temperature variation. The maximum in ΔT does not exist in sub-critical single-phase free convection of (saturated) liquids.

Acknowledgements

The authors are grateful to Andrea Luke for all roughness measurements and evaluations, to Danijel Ninkovic for his assistance in the experiments, to Deutsche Forschungsgemeinschaft (DFG) for funding most of the experimental equipment, and last but not least, to Solvay Fluor und Derivate GmbH for supplying the refrigerant.

REFERENCES

Bier, K., Goetz, J., Gorenflo, D., 1981. Zum Einfluss des Umfangswinkels auf den Wärmeübergang beim Blasensieden an horizontalen Rohren. Wärme Stoffübertragung 15, 159–169.

Buschmeier, M., Sokol, P., Pinto, A.D., Gorenflo, D., 1994. Pool boiling heat transfer of propane/n-butane mixtures at a single tube with superimposed convective flow of bubbles or liquid. In: Proc. 10th Int. Heat Transfer Conf., Brighton UK, vol. 5, pp. 69–74. cf. also: Sokol, P., 1994. Untersuchungen zum Wärmeübergang beim Blasensieden an Glatt- und Rippenrohren mit grossem Aussendurchmesser. DKV-Forschungsbericht Nr. 46, PhD thesis, Univ.-GH Paderborn; cf. also: Buschmeier, M., 1999. Zum Wärmeübergang beim Blasensieden von Propan/n-Butan-Gemischen an einem horizontalen Verdampferrohr mit Queranströmung. PhD thesis, Univ.-GH Paderborn.

Danger, E., 2004. Wärmeübergang und Blasenbildung beim Sieden. DKV-Forschungsbericht Nr. 70, PhD thesis, Univ. Paderborn.

Gorenflo, D., Kenning, D.B.R., 2010. Pool boiling. In: VDI Heat Atlas. Springer-Verlag, Berlin, Heidelberg (Chapter H2).

Gorenflo, D., Baumhögger, E., Windmann, Th., Herres, G., 2010. Nucleate pool boiling, film boiling and single-phase free convection at pressures up to the critical state. Part I: Integral heat transfer for horizontal copper cylinders. Int. J. Refrigeration 33 (7), 1229–1250.

Hahne, E., Barthau, G., 2006. Heat transfer and nucleation in pool boiling. Int. J. Therm. Sci. 45, 209–216.

Hübner, P., Gorenflo, D., Luke, A., 2001. Circumferential temperature distributions on plain and finned tubes in pool boiling. In: Proc. 3rd Conf. Compact Heat Exchangers, Davos, CH, pp. 383–390; cf. also: Hübner, P., 2000. Zum Wärmeübergang beim Blasensieden an Rippenrohren. PhD thesis, Univ.-GH Paderborn.

Kaupmann, P., 1999. Durchmessereinfluss und örtlicher Wärmeübergang beim Blasensieden an horizontalen Stahlrohren. PhD thesis, Univ.-GH Paderborn.

Kenning, D.B.R., Bustnes, O.-E., 2009. Liquid crystal studies of sliding vapour bubbles. Heat Mass Transf. 45, 867–880.

Kotthoff, S., 2010. Zum Einfluss von Fluid- und Heizflächeneigenschaften auf Wärmeübergang und Blasenbildung beim Sieden. PhD thesis, Univ. Paderborn (in preparation).

Kotthoff, S., Gorenflo, D., 2009. Heat transfer and bubble formation on horizontal copper tubes with different diameters and roughness structures. Heat Mass Transf. 45, 893–908.

Kotthoff, S., Gorenflo, D., Danger, E., Luke, A., 2006. Heat transfer and bubble formation in pool boiling: effect of basic surface modifications for heat transfer enhancement. Int. J. Therm. Sci. 45, 217–236.

Luke, A., 2006. Preparation, measurement and analysis of the microstructure of evaporator surfaces. Int. J. Therm. Sci. 45, 237–256.

Ninkovic, D., 2008. Zum Wärmeübergang beim Blasensieden des Kältemittels R125 bei tiefen Temperaturen und Vergleich mit Daten anderer Stoffe. Diplomarbeit, Lehrstuhl f. Thermodynamik und Energietechnik, Univ. Paderborn.

Windmann, Th., 2008. Zum Wärmeübergang beim Blasensieden des Kältemittels R125 bei hohen Drücken bis in die Nähe des kritischen Zustandsgebiets. Diplomarbeit, Lehrstuhl f. Thermodynamik und Energietechnik, Univ. Paderborn.